Computer Vision and Image Understanding **86,** 52–78 (2002)
doi:10.1006/cviu.2002.0958

A Machine Vision System for Lane-Departure Detection

Joon Woong Lee

Department of Industrial Engineering, College of Engineering, Chonnam National University
300, Yongbong-dong Buk-gu, Kwangju, Korea
E-mail: joonlee@chonnam.ac.kr

Received December 20, 2000; accepted March 1, 2002

This paper presents a feature-based machine vision system for estimating lane-departure of a traveling vehicle on a road. The system uses edge information to define an edge distribution function (EDF), the histogram of edge magnitudes with respect to edge orientation angle. The EDF enables the edge-related information and the lane-related information to be connected. Examining the EDF by the shape parameters of the local maxima and the symmetry axis results in identifying whether a change in the traveling direction of a vehicle has occurred. The EDF minimizes the effect of noise and the use of heuristics, and eliminates the task of localizing lane marks. The proposed system enhances the adaptability to cope with the random and dynamic environment of a road scene and leads to a reliable lane-departure warning system.

Key Words: lane-departure detection; image processing; edge distribution function; symmetry axis; departure measure.

1. INTRODUCTION

In this paper, a machine vision system to estimate lane-departure of a traveling vehicle on motorways and similar roads is proposed. A lane-departure warning system (LDWS) prevents dangerous driving situations due to a vehicle's unintentional deviation from the center of its traveling lane. The unexpected lane-departure usually happens because of the temporary and involuntary fade of a driver's vision caused by falling asleep, fatigue, using a mobile phone, operating devices on the instrument panel of a vehicle, chatting, etc. In recent years, automatic detection of lane-departure has attracted much attention because many traffic accident fatalities are related to unintended lane-departures.

An LDWS is different from an autonomous driving system (ADS). The both have their own purpose. The ADS actively guides the vehicle along a lane by steering control as done by Dickmanns [17, 18]. The ADS, in principle, does not allow the deviation of the vehicle

1077-3142/02 $35.00

from the center of its travelling lane and requires precise lane-related information such as a lateral offset of the vehicle relative to lane marks, curvature, and position. In addition, the ADS usually relies on lane tracking. On the other hand, the LDWS only assists the human driver, who drives the vehicle, and passively responds to the circumstance of the vehicle. In the LDWS, it is important to identify whether the lane-departure occurs. Therefore, the LDWS does not necessarily need the offset, curvature and position data, and tracking algorithm.

Most paved roads in Korea have lane marks painted in white, yellow, and even blue. Therefore, identifying lane-departures based on the information of lane marks cannot help depending on image processing techniques even though their robustness is affected by factors of noise that make lane marks invisible even to the human eye. Such factors include corrupted road surfaces such as the wear of painted marks, marks covered by dust or mud, unpredictable weather conditions, illumination changes such as darkness, and various road types such as narrow, wide, curved, straight, inclined, declined, or a tunnel. Much research about road-lane recognition by image processing has been conducted. From such research, feature-based methods [3, 10, 11, 17, 18], neural network-based methods [4, 5], and probabilistic methods [14] have been developed. Most research shares and combines various principles from these methods. One common issue in these methods is how to provide a reliable algorithm because most methods are influenced by noise. Extraction of lane-related information is usually the first step of lane-departure detection.

Measuring the relative position between lane marks and a vehicle has been a well-known method for the design of lane-departure detection because of its simple concept [3, 7, 9, 11]. This method relies on the precise localization of lane marks to obtain the offset between the center of the lane and the center axis of the car body. However, the position of lane marks is often accompanied by an error because sources of noise lead to false alarms and miss-detections. This method often needs camera calibration to obtain the geometric model of the camera and road surface, and widths of both the vehicle and the lane. Therefore, the method is affected by several parameters—the selection of a camera, lens optics, the mounting position of the camera, the type of road, and the subject vehicle. From this point of view, the RALPH [3] can be considered a similar approach to this method.

In this paper, lane-departure detection is conducted by measuring the orientation of lane marks in gray-level images taken by a CCD camera mounted on a test vehicle. The phenomena that occurred from lane-departure are discovered through the deliberate experiments. The pictorial description of lane-departure of a vehicle is shown in Fig. 1a. When the traveling direction of a vehicle deviates from the center of its traveling lane in the left or right direction, the orientation of lane boundaries changes as shown in Figs. 1b and 1c. Based on this knowledge, the proposed method focuses on measuring the change in orientation of lane marks to determine whether the lane-departure occurs. Different from the extraction of positional offset between lane boundary and a vehicle as done by Pomerleau and Jochem [3] and Dickmanns and Zapp [18], the proposed approach is not influenced by the parameters of lens optics, width of the traveling lane, vehicle type, and the localization of lane marks.

In order to realize the proposed method, the assumptions of lane marks on roads are established: (1) Lane marks are painted in a brighter color than other parts, (2) the orientation of lane marks changes are small and smooth along the lane, and (3) lane marks are parallel to left and right from the center of the lane. These assumptions can be thought of as the properties of lane marks. Based on the assumptions, an edge distribution function (EDF) as a one-dimensional function is defined. Formulated by accumulating the edge magnitude of

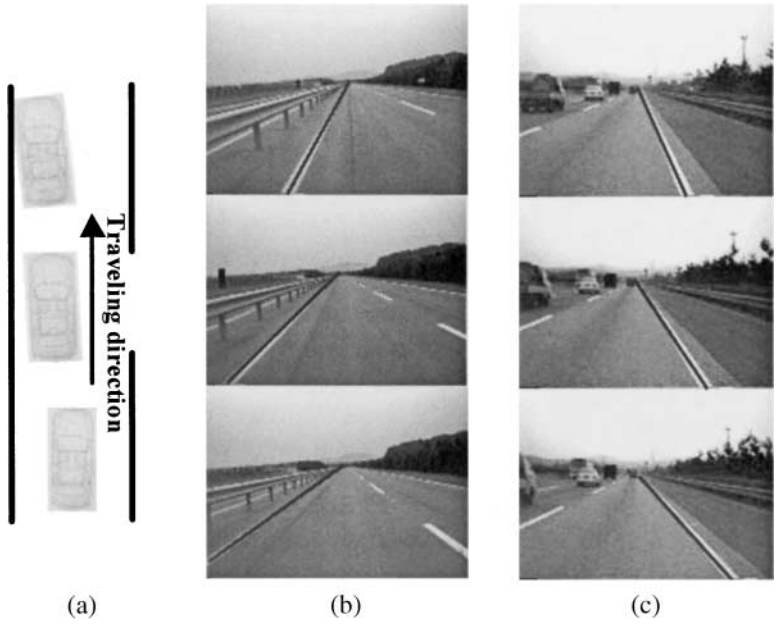

FIG. 1. The description of a lane-departure. (a) Description of lateral deviation of a traveling vehicle. (b) Change in orientation of lane marks when a vehicle approaches the left direction. (c) Change in orientation of lane marks when a vehicle approaches the right direction.

pixels of the same edge orientation in the region of interest, EDF plays four important roles. (1) It reduces the noise-related effects of a dynamic road scene. (2) It makes possible the measuring of a lane orientation without camera-related parameters. (3) It makes the lane-departure alert problem to a mathematical one by using its two important shape features—local maxima and a symmetry axis. (4) It enables the edge-related information and the lane-related information to be connected.

The third assumption of parallelism can be analyzed by the EDF. Mathematically, a signal or function can be decomposed into even and odd functions. Its symmetry measure is expressed by the respective energy contents of the decomposed functions as done by Zielk *et al.* [1]. Using this principle, the symmetry axis of the EDF is extracted. The axis is used to estimate lane-departure because the location of the axis changes when a vehicle deviates from the center of its traveling lane. In addition, according to the first two assumptions, the EDF has distinctive peak values at the locations corresponding to the orientation of lane boundaries. Accordingly, the local maxima of the EDF are estimates of the orientation of lane boundaries. The symmetry axis and the local maxima consequently work in cooperation to identify lane-departure. In the EDF-based lane-departure detection system, road shapes such as inclined, declined, wide, and narrow, vehicle types, and the number of occupants do not affect the algorithm.

The EDF constructed by road images that do not satisfy three assumptions of lane boundary may not provide distinctive peak points. For example, the EDF from a curved road with a small radius of curvature such as a ramp or a rural narrow road may not guarantee the existence of distinctive peak points. However, highways in Korea are designed to have at least the minimum radius of curvature of 280 m, in which the influence of lane curvature is

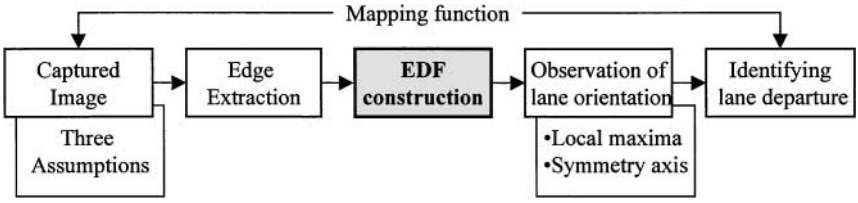

FIG. 2. Basic procedure of lane departure detection.

negligible at near distances of about 40 m as indicated by Dickmanns [18]. Eventually, the EDF of a highway image is available for the detection of lane-departure even though the lane direction is curved.

The proposed algorithm is largely structured in three steps. Figure 2 illustrates the basic procedure. The first step is image acquisition and edge extraction. The second step is EDF formulation and estimation by a moving sum-based recursive filter. The last step is searching the local maxima and symmetry axis of the EDF. In the lane-departure alert system, of importance is measuring the vehicles' signals such as velocity, steering angle, braking on and off, wiper on and off, and turn signal to determine the driver's intention to change lanes and his or her alertness. However, we do not deal with that issue in this paper.

2. EDF

2.1. Region of Interest

If a CCD camera is mounted on a test vehicle such that the optical axis coincides with the centerline of the car body, and roll and tilt angles are 0°, the vanishing point of the road images appears in the center of the vertical direction. Then it is necessary to limit the processing area below the vanishing point because lanes visible in a road image generally lie in that area. In addition, we assume that there is no horizon or vertical lane in the images. In fact, there are no visible lanes in the horizon except for a steep curved road. Depending on the constraint of camera mounting, the region of interest (ROI) for image processing is confined within the shaded regions as shown in Fig. 3. There are two purposes for the construction of the ROI: (1) To reduce processing time, and (2) to highlight the ROI with respect to a traveling lane.

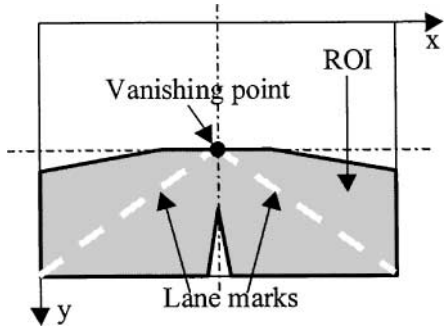

FIG. 3. ROI for image processing.

2.2. Edge Extraction

The reasons the edge is selected as the image-primitive are: (1) the most distinctive edge pixels appear along lane boundaries in a road image, and (2) the edge itself has directional information that correlates with lane orientation.

An edge is mathematically defined by the gradient of the intensity function. At a point (x, y) of an image $f(x, y)$, the gradient is represented by a vector $\nabla \mathbf{f}$ as follows:

$$\nabla \mathbf{f} = [G_x \quad G_y]^T = \left[\frac{\partial f}{\partial x} \quad \frac{\partial f}{\partial y}\right]^T. \tag{1}$$

The vector has two important physical quantities, magnitude $\nabla f(x, y)$ and orientation $\alpha(x, y)$, as shown below:

$$\nabla f(x, y) = \sqrt{G_x^2 + G_y^2} \approx |G_x| + |G_y| \tag{2}$$

$$\alpha(x, y) = \tan^{-1}\left(\frac{G_y}{G_x}\right). \tag{3}$$

In order to reduce the processing time for calculating $\alpha(x, y)$, a simple look-up table (LUT) of edge direction was constructed in advance. G_x and G_y at relevant pixels index directly to the associated label. Depending on the range of G_x and G_y, and the quantization level of $\alpha(x, y)$, the size of the LUT was determined. In an edge operation, choosing a threshold value for edge magnitude is a difficult problem [12]. While the pixels from lane boundaries in a road image have a large magnitude, their numbers are small compared with other pixels. Therefore, it is necessary to eliminate pixels with small magnitude to raise the effect of pixels from lane boundaries. An adaptive method from [16] was used to determine the threshold.

2.3. EDF

2.3.1. Construction. Based on edge information and the three assumptions of lane marks on roads, an EDF is defined as the one-dimensional function

$$F(d) = \sum_{n(d)} \nabla f(x, y), \tag{4}$$

where $n(d)$ is the number of pixels with orientation $d = \alpha(x, y)$ of Eq. (3), and $\nabla f(x, y)$ is the edge magnitude of Eq. (2). To obtain $n(d)$, we set the range of $\alpha(x, y)$ as 0° to 180° and use a quantization of 1°. The EDF is the histogram of the edge magnitude of pixels with respect to the orientation. In addition, it connects the edge-related information to the lane-related information. It provides two important shape features: the local maxima and the symmetry axis. The graphical form of an EDF is shown in Fig. 4b, in which the local maxima exist near θ_1 and θ_2 that correspond to the directions of right and left lane boundaries, respectively. A symmetry axis of the EDF is generally located near 90°.

2.3.2. Local maxima and symmetry axis. If we carefully look at the EDF, we notice there are two important facts. (1) EDF has large values in the vicinity of lane directions. This is basically caused by the first two assumptions of lane marks as explained in Section 1.

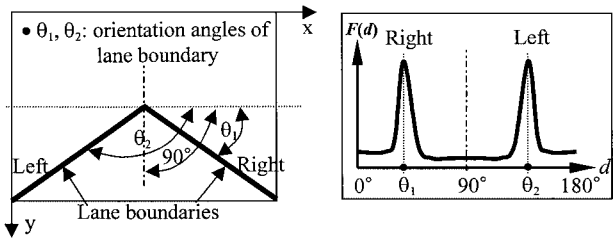

FIG. 4. (a) Orientation angle of lane boundary, and (b) EDF.

There seldom exists a mark or objects satisfying three assumptions except for lane marks. These facts cause the EDF to have the local maxima near the directions θ_1 and θ_2 of the right and left lanes of road images. (2) An axis dividing the EDF into left and right symmetry is highly correlated with the location of the image-capture. If a road image is taken at the center of the lane, the symmetry axis will be located near 90°. On the other hand, if the position of the image-capture is deviated from the center of the lane, the location of the symmetry axis also deviates from 90°. This fact originates from the third assumption of lane marks.

2.4. Recursive Filter of EDF

It is often difficult to infer the lane direction by the local maxima of $F(d)$ due to the effects of noise. In this section, an accumulation-based method is introduced to minimize the temporal effects of noise. Even if a good signal among noisy corrupted signals is buried in the accumulation, the accumulation in general reduces the temporal effects of noise. For a sequence of successive N images, the accumulation of $F(d)$ of each frame provides a new estimator of the EDF defined by

$$\hat{H}_{\mathrm{k}}(d) = \sum_{\mathrm{i=k-N+1}}^{\mathrm{k}} F_i(d), \qquad k \geq N, \tag{5}$$

where k represents the current frame. Here, N is determined experimentally. Based on a moving sum, the estimator $\hat{H}_{\mathrm{k}}(d)$ is redesigned to a recursive form as follows:

$$\hat{H}_{\mathrm{k}}(d) = \hat{H}_{\mathrm{k-1}}(d) - F_{\mathrm{k-N}}(d) + F_{\mathrm{k}}(d), \qquad k \geq N + 1. \tag{6}$$

This recursive filter has two advantages. (1) It takes less processing time than the accumulation of Eq. (5). (2) While a Kalman filter-based recursive filter [13] diverges or converges very slowly to the steady state when the transition from an assumed state occurs, the filter of Eq. (6) converges to the steady state without divergence. In a Kalman filter-based recursive filter, the Kalman gain becomes small when a steady state is reached. If a transition occurs from this steady state, the filter cannot follow the transition state even though the measurement residual becomes large.

For example, let us assume a filter similar to the Kalman filter,

$$\hat{H}_{\mathrm{k+1}}(d) = \hat{H}_{\mathrm{k}}(d) + K_k(F(d) - \hat{H}_{\mathrm{k}}(d)), \tag{7}$$

where K_k is the gain and $F(d) - \hat{H}_k(d)$ is the measurement residual. If a vehicle travels at the center of the traveling lane, the EDFs of both filters of Eqs. (6) and (7) have similar shapes as shown in Fig. 4b. However, if the vehicle starts to lane-change, the filter of Eq. (7) cannot track the change. As shown in [16], after the lane-change is completed, the filter of Eq. (7) does not recover the shape of EDF. Therefore, in a traffic scenario, the moving sum-based filter of Eq. (6) is more acceptable.

3. SYMMETRY MEASURE OF EDF

A function $f(x)$ is represented by the sum of the even function $f_e(x)$ and odd function $f_o(x)$. Each of them is expressed by

$$\begin{aligned} f_e(x) &= \frac{f(x) + f(-x)}{2}, \qquad x \in (-\varphi/2, \varphi/2) \\ f_o(x) &= \frac{f(x) - f(-x)}{2}, \qquad x \in (-\varphi/2, \varphi/2), \end{aligned} \tag{8}$$

where φ is the range in which $f(x)$ is defined. The even function has the property of symmetry of an axis and the odd function has the property of symmetry of an origin. Here, we are interested in the property of symmetry of an axis.

- Searching interval of the symmetry axis

As referred to in Section 2.3, if a road image is taken at the center of the lane, the symmetry axis will be located near 90°. On the other hand, if a vehicle deviates from the center of the traveling lane, the symmetry axis correspondingly deviates from 90°. According to this fact, the searching interval β of the symmetry axis will be selected as $90^\circ - \gamma \le \beta \le 90^\circ + \gamma$, where γ is selected experimentally to know the position of the symmetry axis even in the situation of a lane-change.

- Evaluation interval of EDF to search for the symmetry axis

Even though the inside angle of the subject lane, that is, $\theta_2 - \theta_1$ in Fig. 4a, depends on lens optics, we consider the inside angle to be within 150°. Accordingly, the evaluation interval w of a symmetry axis is set to 150°, which takes less processing time than the interval of 180°.

- Symmetry measure

We define the even and odd functions of $F(d)$ for a given interval of width w about x_s such that

$$\begin{aligned} F_e(x_s + x) &= \begin{cases} \frac{F(d) + F(-d)}{2}, & \text{if } d \in (0, w/2), \quad x_s \in \beta \\ 0, & \text{otherwise} \end{cases} \\ F_o(x_s + x) &= \begin{cases} \frac{F(d) - F(-d)}{2}, & \text{if } d \in (0, w/2), \quad x_s \in \beta \\ 0, & \text{otherwise.} \end{cases} \end{aligned} \tag{9}$$

Using the subtitution $x = d - x_s$, we can shift the origin of $F(d)$ to any position x_s which may be thought of as denoting the location of a potential symmetry axis with w being the width of the symmetric interval. We account for the significance of $F_e(x_s + x)$ and

$F_o(x_s + x)$ by their respective energy contents using the energy function. Using an idea performed by Zielk *et al.* [1], a symmetry measure $S(x_s, w)$ representing the degree of symmetry for any potential symmetry axis at x_s with respect to an evaluating interval w is defined as

$$S(x_s, w) = \frac{\int_0^{w/2} |F'_e(x_s + x)|^2\, dx - \int_0^{w/2} |F_o(x_s + x)|^2\, dx}{\int_0^{w/2} |F'_e(x_s + x)|^2\, dx + \int_0^{w/2} |F_o(x_s + x)|^2\, dx}, \qquad -1 \le S(x_s, w) \le 1, \quad (10)$$

where $F'_e(x_s + x) = F_e(x_s + x) - \frac{2}{w} \int_0^{w/2} F_e(x_s + x)\, dx$ and the integral of each function represents the energy of the function.

A potential symmetry axis $\hat{x}$ in which the symmetry measure $S(\hat{x}, w)$ has the largest value is selected as the symmetry axis of $F(d)$.

4. ESTIMATION OF LANE DEPARTURE

4.1. Estimation of Lane Departure by the Symmetry Axis

If the symmetry axis $\hat{x}$ is largely apart from 90°, it may be thought of as a lane-departure of the traveling vehicle. To represent the state of lane-departure quantitatively the deviation distance ρ is defined as

$$\rho = |\hat{x} - x_c|, \quad (11)$$

where x_c is the symmetry axis obtained by keeping a vehicle at the center of its traveling lane. Ideally, x_c should be 90°, but in reality it is in the neighborhood of 90° because there may be discord of the optical axis to the center-line of a car body by an offset or a twist. Consider the case of $\rho \ge \varepsilon$ as the lane-departure, in which ε is selected experimentally.

4.2. Estimation of Lane Departure by the Local Maxima

Searching for the local maxima of EDF is implemented by the Lunenberger definition of a "local maximum point" [2]. The departure measure ξ based on the local maxima is defined as

$$\xi = \frac{d_l^* - x_c}{x_c - d_r^*}, \quad (12)$$

where d_l^* and d_r^* are the detected local maxima which correspond to the estimates of directions θ_1 and θ_2 of the right and left lane boundaries as shown in Fig. 4b, respectively, and x_c is the same as in Eq. (11). If the measure ξ is close to 1, it can be considered that a vehicle keeps well to the center of its traveling lane. If $\xi \ge \eta_1$ or $\xi \le \eta_2$ is proven, it is compared to the lane-departure, in which η_1 is a constant greater than one and η_2 is a constant less than one. Both values are selected experimentally.

5. EXPERIMENTAL RESULTS

The proposed system was evaluated with images captured by a CCD camera mounted on a vehicle [15]. Road tests were conducted at highways paved with asphalt and cement

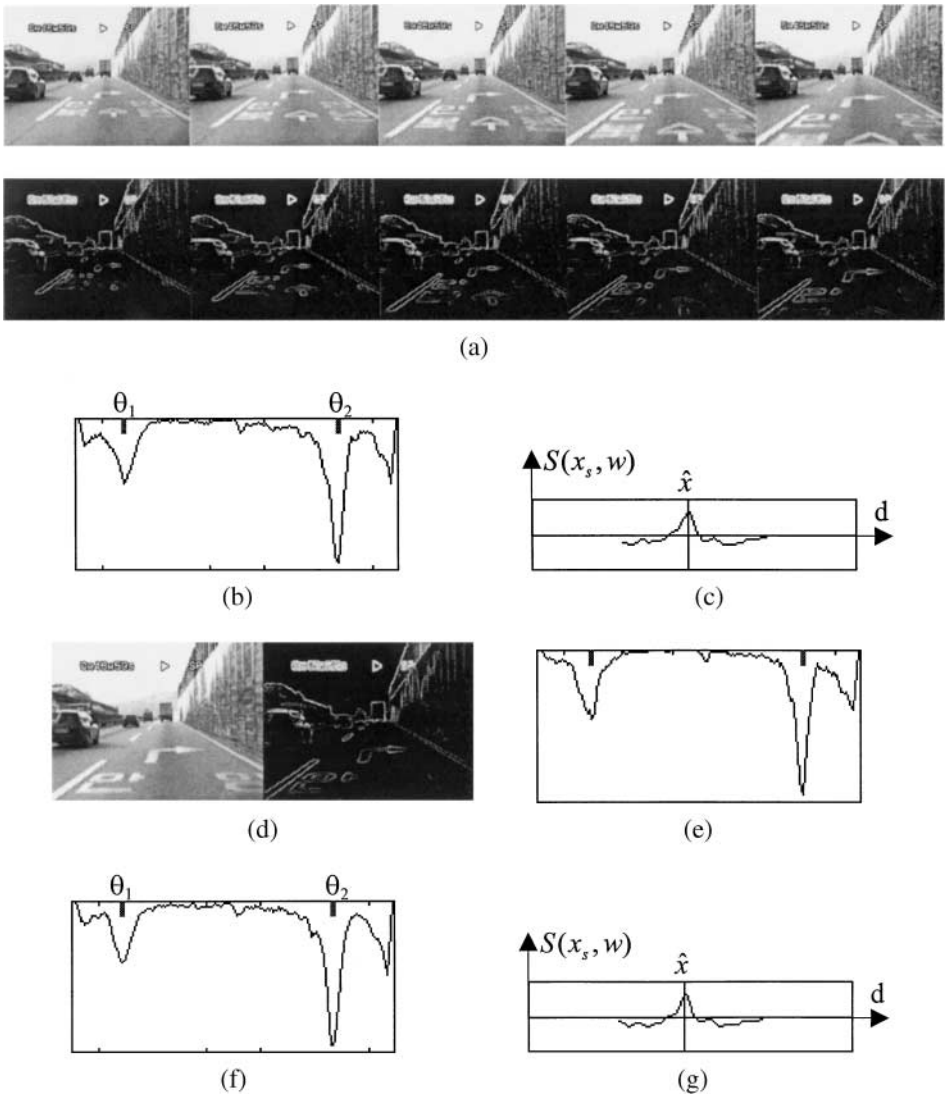

FIG. 5. General procedure of the proposed algorithm. (a) Successive gray-level images and their edge images. (b) $\hat{H}(d)$ and its local maxima. (c) Symmetry measure of $\hat{H}(d)$. (d) New input image and its edge image. (e) $F(d)$ of new input image. (f) New $\hat{H}(d)$ and its local maxima. (g) Symmetry measure of new $\hat{H}(d)$.

while driving a test vehicle at a velocity about 100 km/h. Lab tests were also carried out by recording the video sequences of road scenes. In the tests, the image size was 160×120 (pixels), the number of image sequences used in Eq. (5) was five, and a 3×3 Sobel edge operator [8] was used to extract edges.

The general procedure of the proposed algorithm is presented by experimental results as shown in Fig. 5. Figure 5a shows the five successive gray-level images and their edge images. Figure 5b shows the estimated EDF $\hat{H}(d)$ of Eq. (5) and its local maxima $\theta_1 = 27$ and $\theta_2 = 146$. Figure 5c shows the plots of symmetry measure and symmetry axis $\hat{x} = 86^\circ$. Experimentally, we found $x_c = 88^\circ$ and obtained the deviation distance $\rho = 2$ and the departure measure $\xi = 1.05$. Figure 5d shows a new image and its edge image and Fig. 5e shows the EDF $F(d)$ for the new image. By the recursive filter of Eq. (6), the EDF $\hat{H}(d)$ is

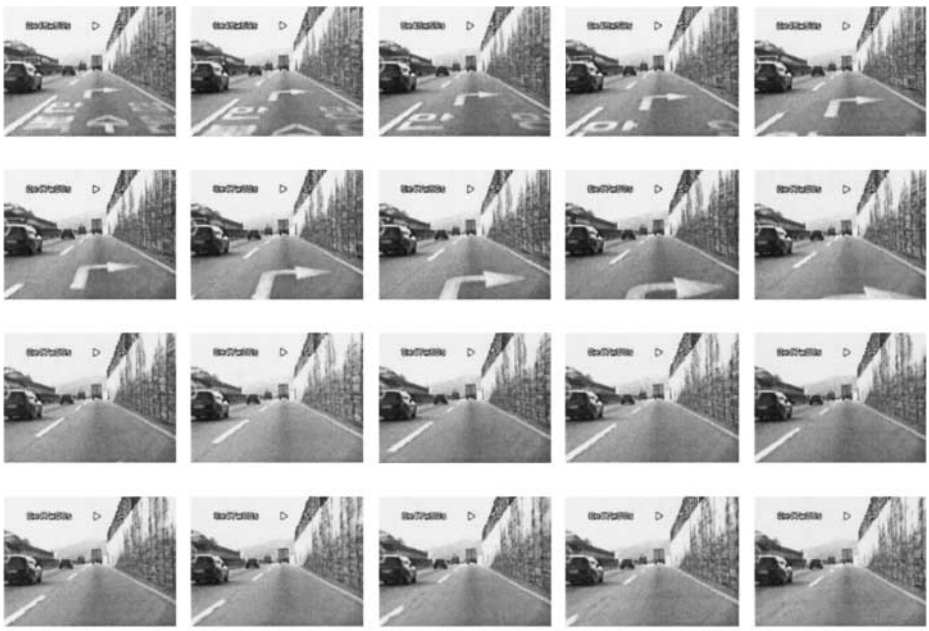

(a)

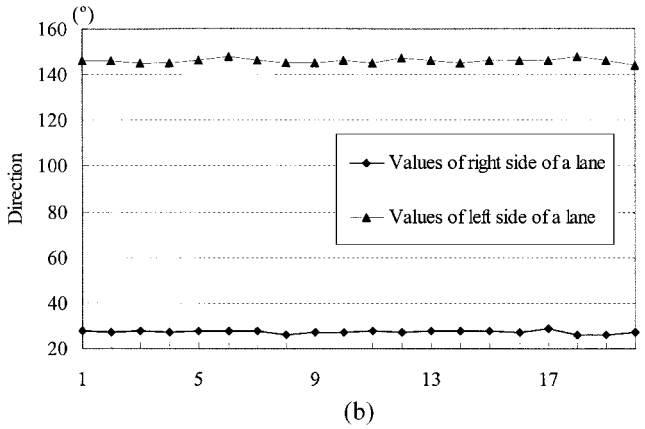

(b)

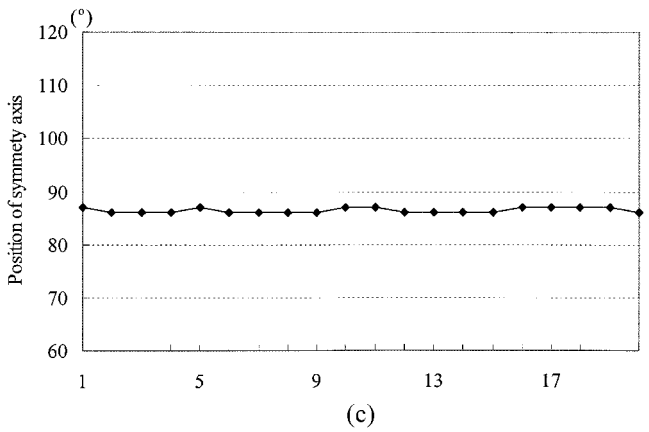

(c)

FIG. 6. Experimental results in the daytime on a straight road. (a) A series of images. (b) Representation of local maxima as the direction of a lane. (c) Representation of the symmetry axis.

estimated as shown in Fig. 5f. The local maxima of the new $\hat{H}(d)$ are $\theta_1 = 28$ and $\theta_2 = 145$. Figure 5g shows the symmetry measure of the new EDF and its symmetry axis $\hat{x} = 86^\circ$. By the parameters of ρ and ξ, it was known that the vehicle did not deviate from the center of its traveling lane.

Experiments were performed in the daytime and in the nighttime on a straight road. The results are shown in Figs. 6 and 7, respectively. During the tests, there was no lane-departure of a vehicle. The experimental results shown in Figs. 6b and 6c and in Figs. 7c and 7d were consistent with the real situation in which the numbers on the horizontal axis represent

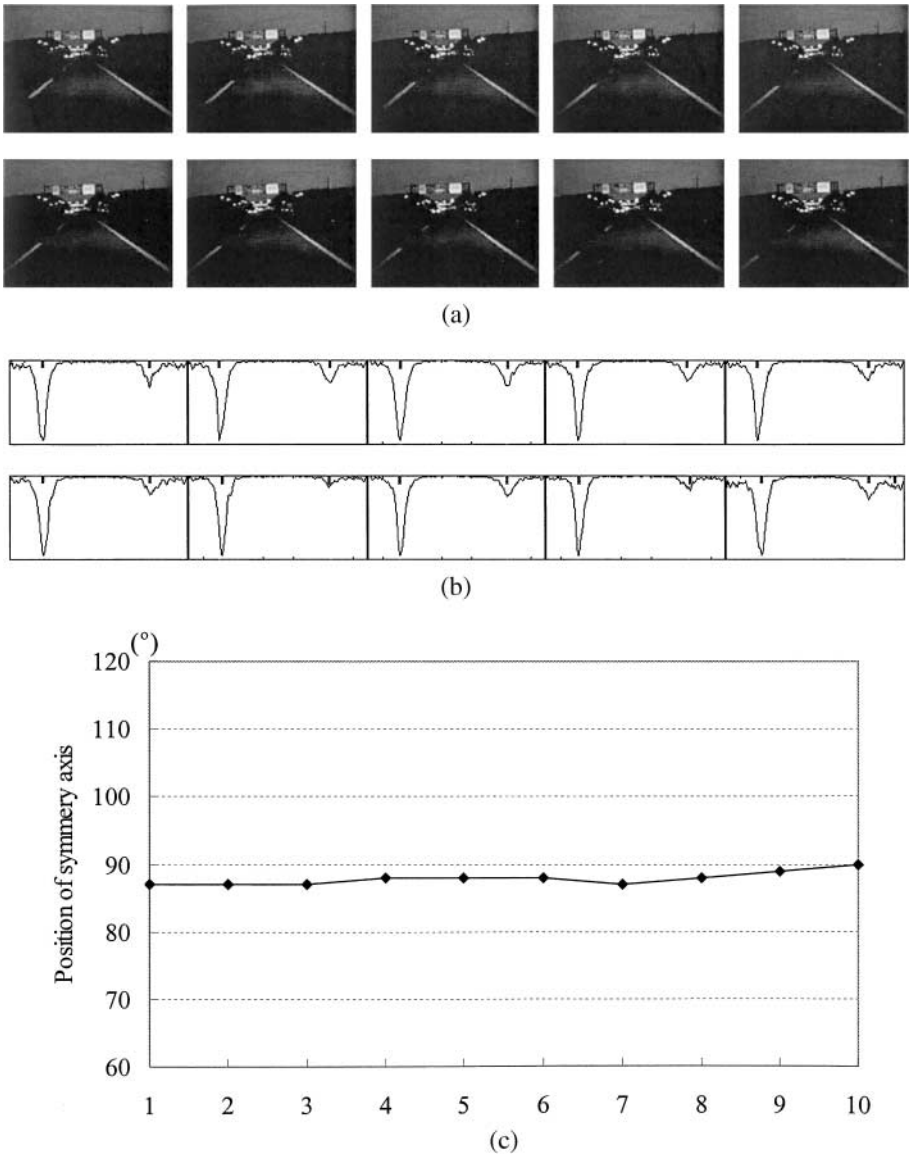

FIG. 7. Experimental results in the nighttime on a straight road. (a) A series of images. (b) EDFs of the series of images shown in (a). (c) Representation of local maxima as the direction of a lane. (d) Representation of a symmetry axis.

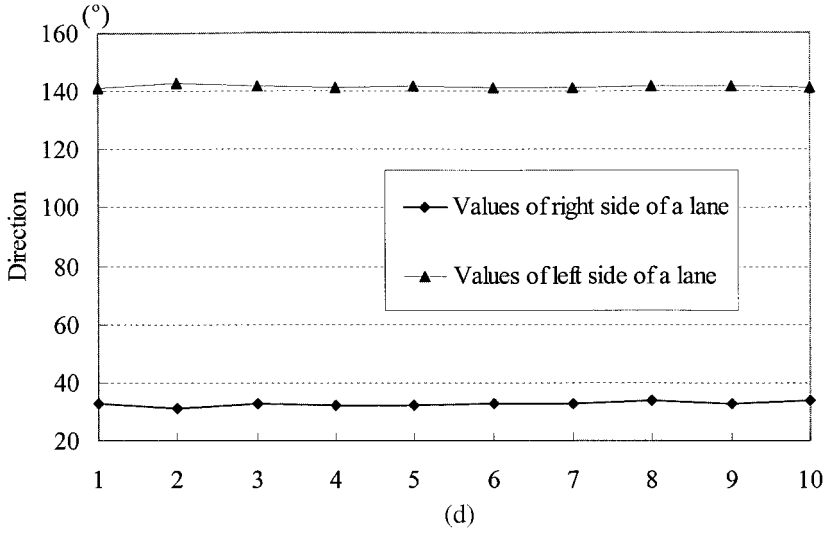

FIG. 7—*Continued*

the frame number of images shown in Figs. 6a and 7a. There was no large variation in the values of the local maxima and the symmetry axis between frames.

The next two experiments were conducted when a lane-departure occurred. Experimental results show that lane-departure can be identified by observing the change in the lane direction. The first experiment was performed when a test vehicle moved to the left side of its traveling lane and returned to the center of the lane. Figure 8a shows a series of images composed of ten frames. Figure 8b shows EDFs for these images and Figure 8c shows the local maxima of the EDFs. In Figs. 8c to 8f, the numbers on the horizontal axis represent frame numbers. The symmetry axis, the deviation distance, and the departure measure were presented in Figs. 8d to 8f, respectively. From the experimental results, one is able to observe that the test vehicle deviates from the center of its traveling lane to the left and returns again to the center of the lane. As the vehicle moves to the left, the locations of the symmetry axis and local maxima also moved to the left on the EDF as shown in Figs. 8b to 8d. The results show that the locations of the symmetry axis and local maxima are highly correlated with the traveling direction of the vehicle. The lane departure is identified by the variations of the parameters of ξ and ρ shown in Figs. 8e and 8f.

Next, we provide the test results performed when the test vehicle moved to the right, crossed the right lane boundary by the front wheel of the vehicle and returned back to the center of its traveling lane. Figure 9a shows a series of images composed of 29 frames. The EDFs for these images were presented in Fig. 9b. From these EDFs, the local maxima and the symmetry axis were extracted, and the departure measure and deviation distance were computed. In Figs. 9c to 9f, the numbers on the horizontal axis represent the image numbers. The local maxima, the symmetry axis, the deviation distance, and the departure measure were presented in Figs. 9c to 9f, respectively. From these figures, one notices that as the vehicle approaches close to the lane on the right side, the departure measure becomes small and the deviation distance becomes large. The timing of the lane-departure warning is determined by the values of ε of Eq. (11) and η_1 and η_2 of Eq. (12). In this experiment, we selected the values $\eta_1 = 1.3$ and $\eta_2 = 0.7$. The warning began on the 13th frame and ended on the 20th frame.

The following experiment was related with a curved road. From the experimental results shown in Fig. 10, we can find the following features. (1) There is a difference in the lane direction of about 5° between a right-curved road and a left-curved road as shown in Fig. 10d. (2) While the locations of the symmetry axis for a right-curved road are generally above 90°, the locations of the symmetry axis for a left-curved road are below 90° as shown in Fig. 10e. (3) While the departure measures for a right-curved road are generally less than 1.0, the departure measures for a left-curved road are greater than 1.0 as shown in Fig. 10f.

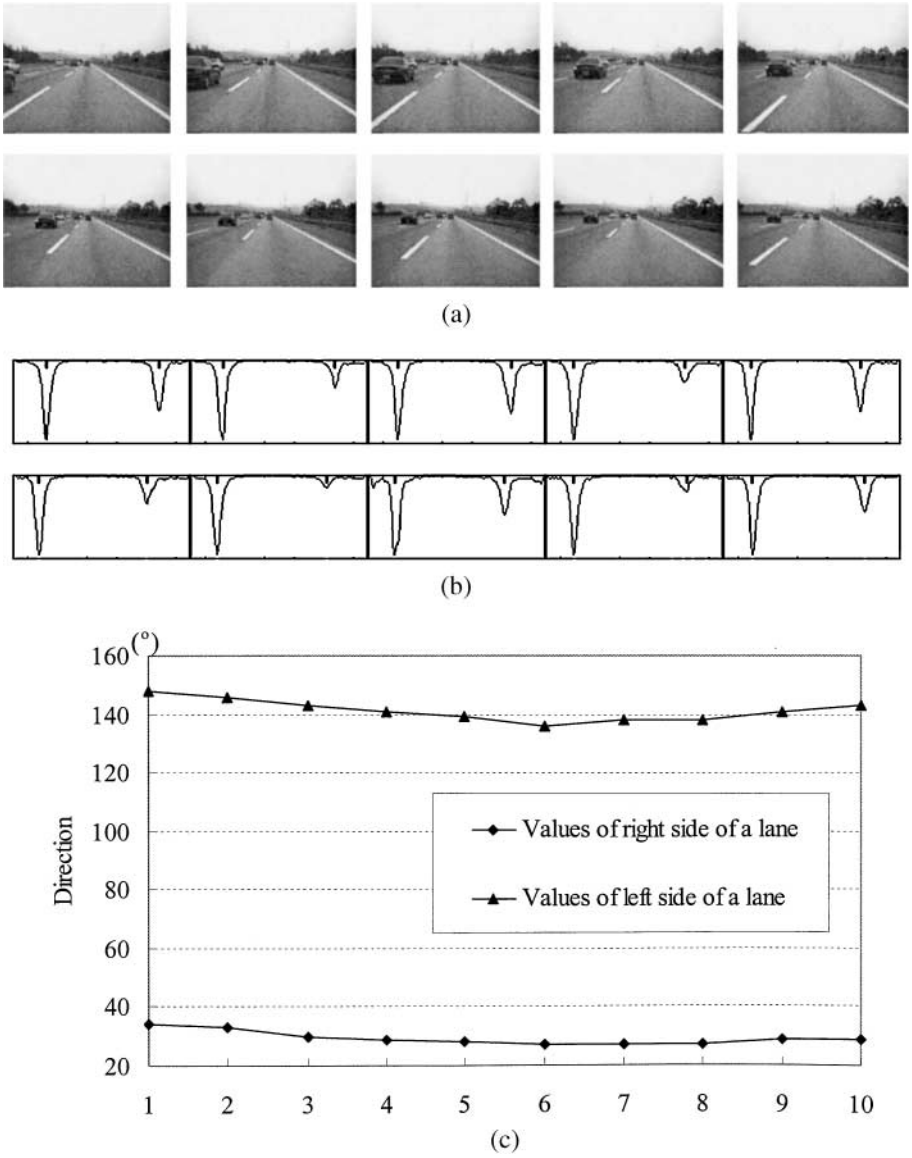

FIG. 8. Experimental results under a lane-departure to the left side. (a) A series of images. (b) EDFs of the series of images shown in (a). (c) Representation of local maxima as the direction of a lane. (d) Representation of the symmetry axis. (e) Departure measure. (f) Deviation distance.

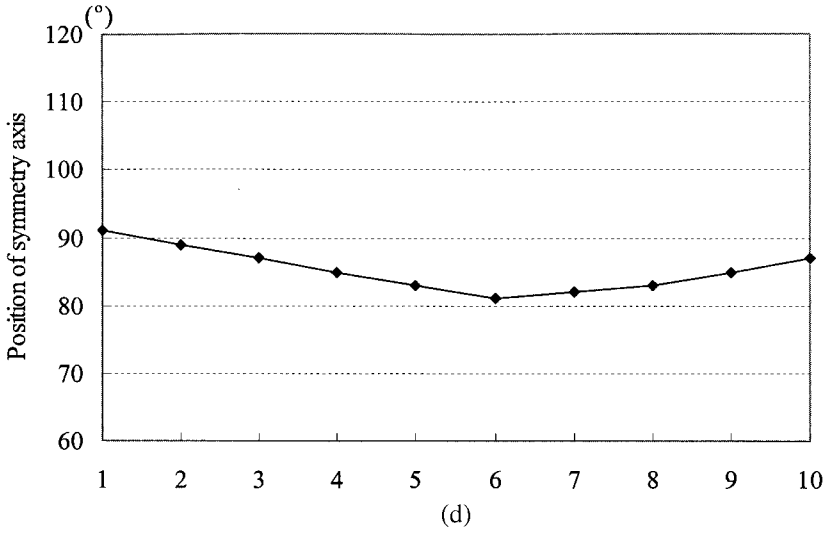

(d)

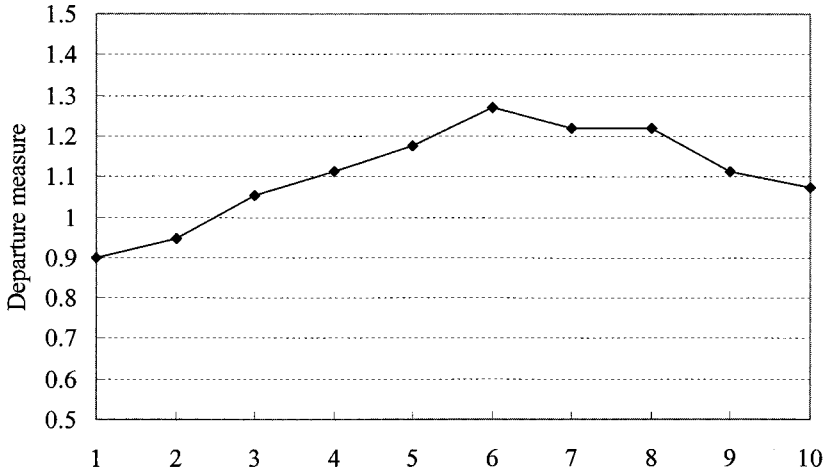

(e)

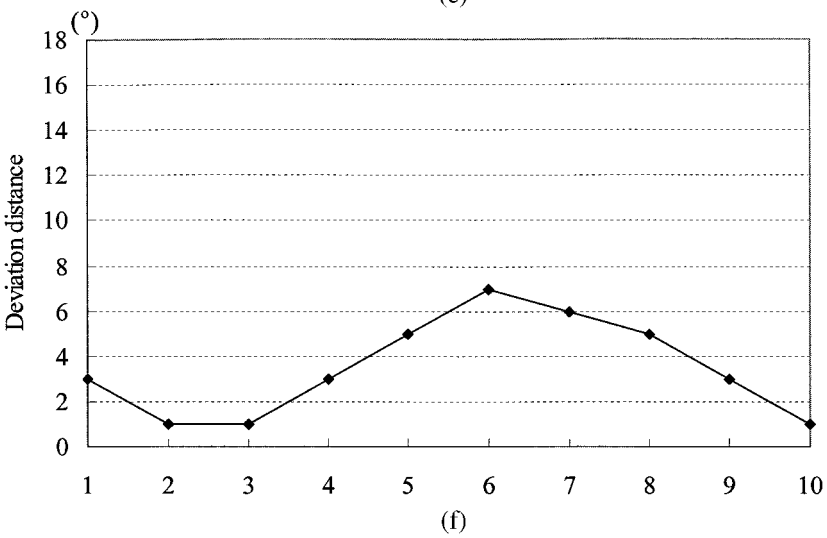

(f)

FIG. 8—*Continued*

Unlike straight roads, a false alarm or a miss-detection of lane departure on curved roads may occur due to the self-change in lane orientation. From Fig. 10f, the 2nd to 5th and 18th to 20th image frames on the right-curved road, and the 5th to 6th and 14th to 19th frames on the left-curved road could be regarded as lane departure depending on the choice of η_1 and η_2 of Eq. (12).

6. DISCUSSION

6.1. Curved Road

Applicability. It is important to evaluate the applicability of the EDF to the LDWS because the EDF as a one-dimensional function does not provide enough information with respect to a curvature. Specifications of the Korean road structure and its facility criterion are shown in Table 1. They are important parameters.

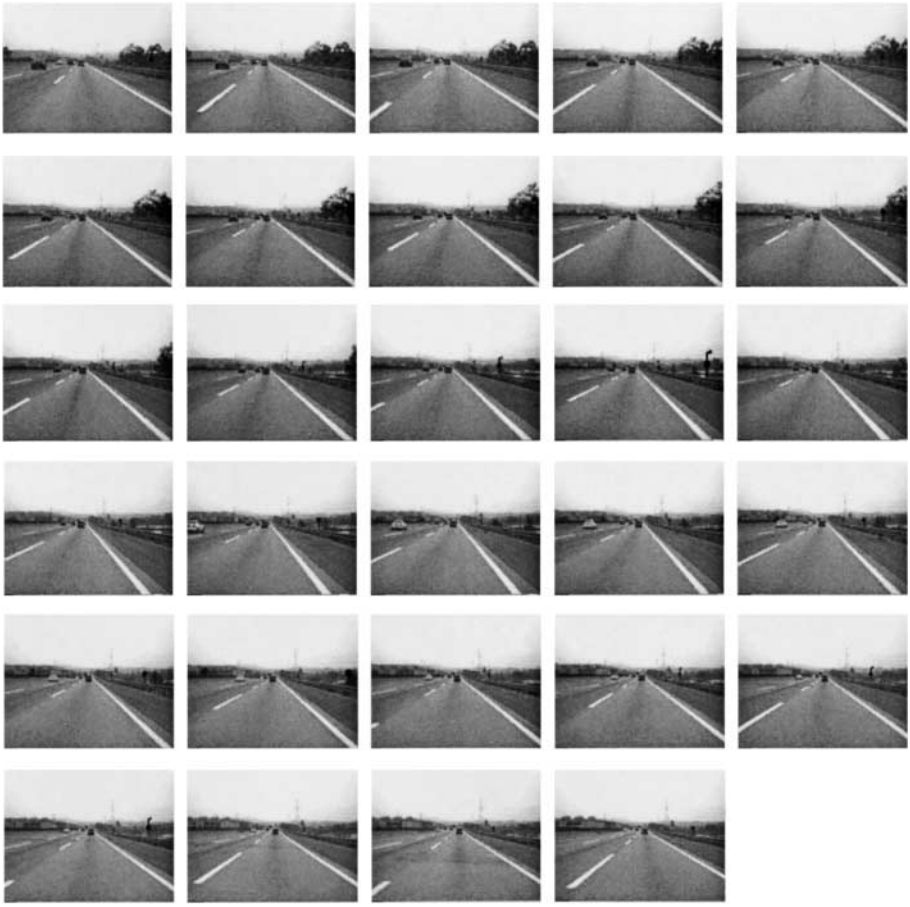

FIG. 9. Experimental results under a lane departure to the right side. (a) A series of images showing a deviation. (b) EDFs of the series of images shown in (a). (c) Representation of local maxima as the direction of a lane. (d) Representation of the symmetry axis. (e) Departure measure. (f) Deviation distance.

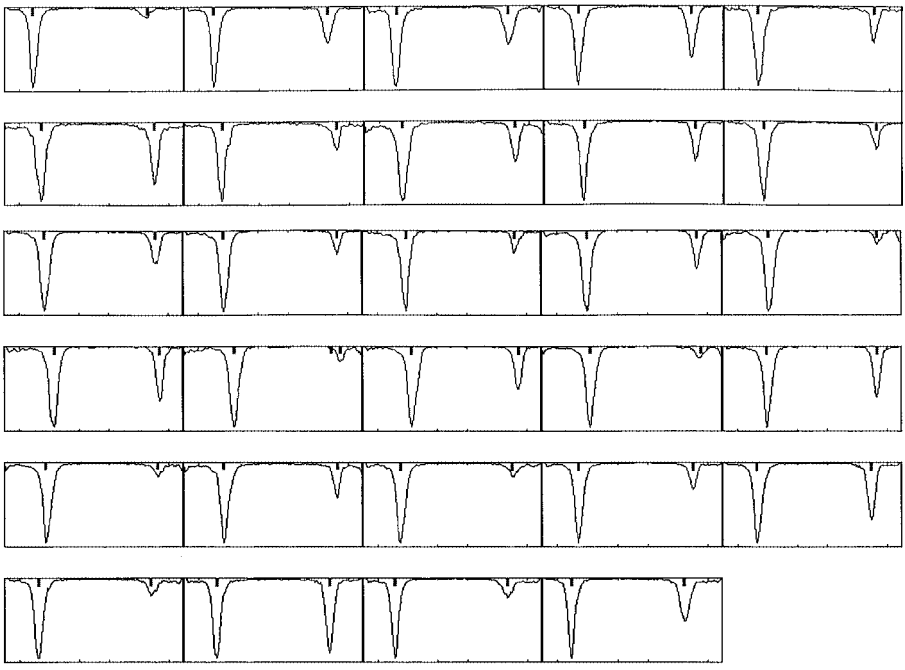

(b)

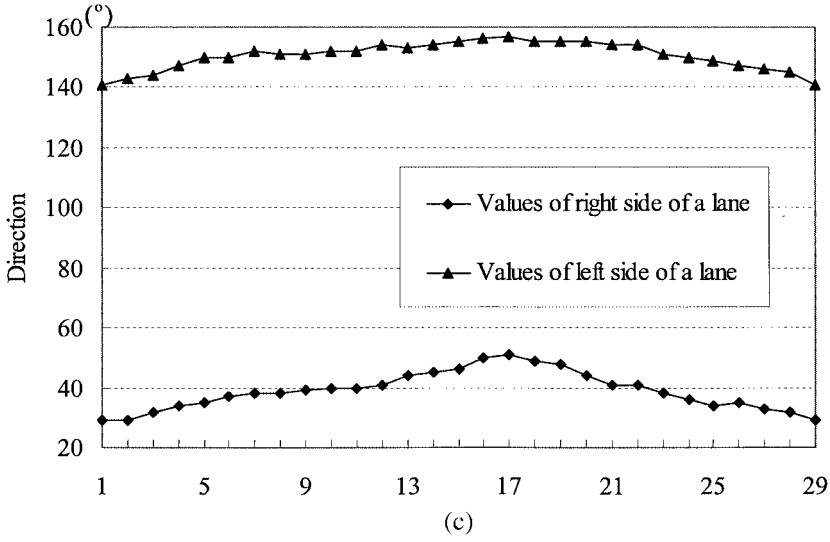

(c)

FIG. 9—*Continued*

Assuming that the focusing distance for driving a vehicle is within 40 m, then 40 m is the length of the chord for each type of road in Table 1. The distances to the chord of the arc from the center of the circle are 709.72 m for the type-1 road, 459.57 m for the type-2 road, 279.29 m for the type-3 road, and 138.56 m for the type-4 road, respectively. Therefore, a road designed for more than 80 km/h can be regarded as straight to some 40 m in front. For a road designed for less than 60 km/h, it is unreasonable to consider some 40 m in front as straight because the difference between the distance to the arc and the distance to the

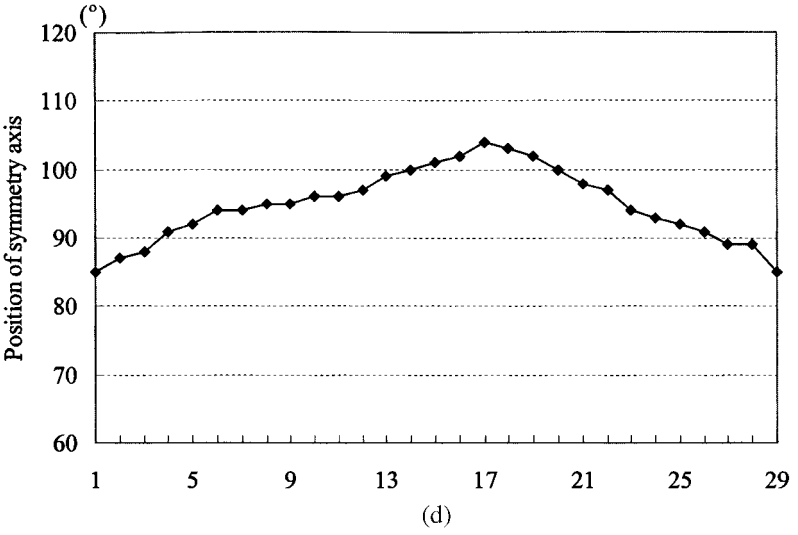

(d)

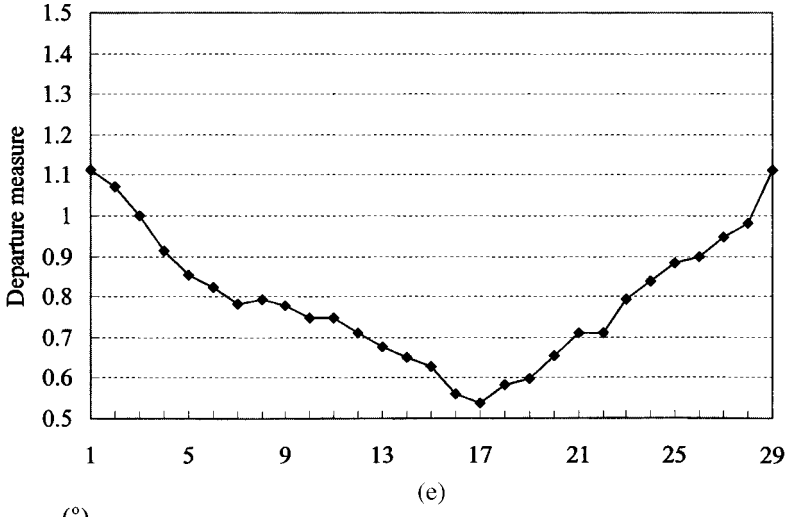

(e)

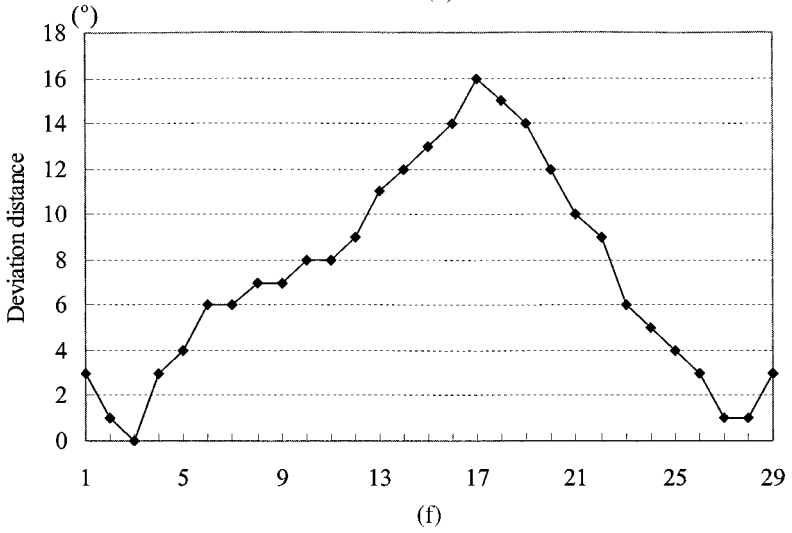

(f)

FIG. 9—*Continued*

TABLE 1
Korean Road Structure and Its Facility Criterion

Type	Designed velocity (km/h)	Minimum radius of curvature (m)	Minimum width (m)
1	120	710	3.5
2	100	460	3.5
3	80	280	3.5
4	60	140	3.25
5	50	90	3

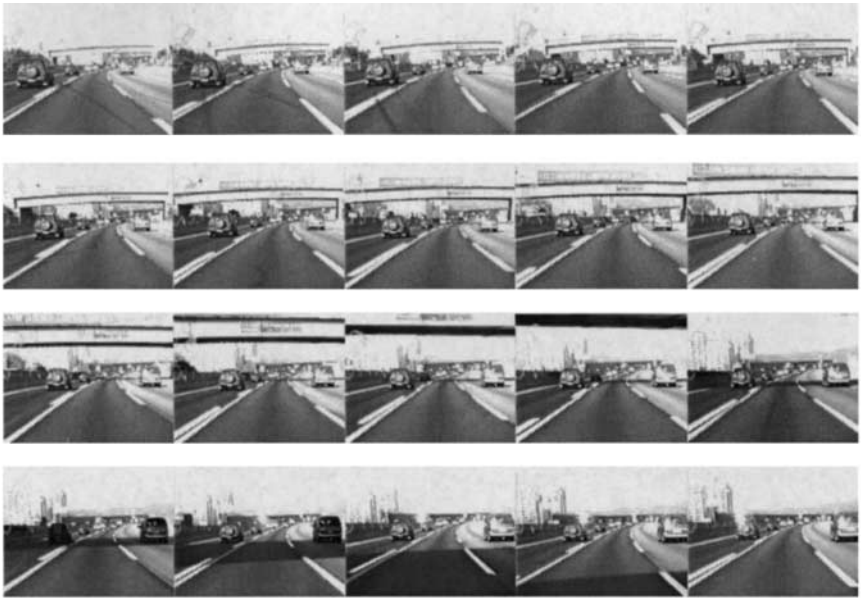

(a)

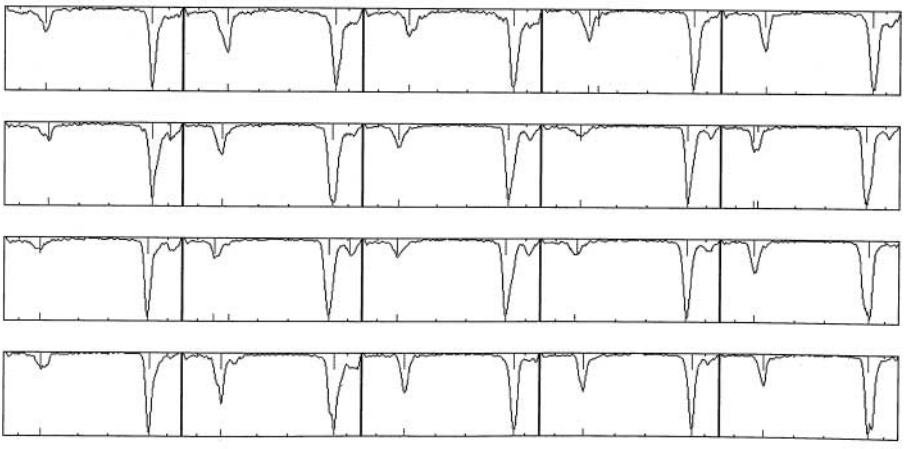

(b)

FIG. 10. Experimental results on curved roads. (a) A series of images captured on a right-curved highway. (b) EDFs of the series of images shown in (a). (c) A series of images captured on a left-curved highway. (d) Representation of local maxima as the direction of a lane. (e) Representation of the symmetry axis. (f) Departure measure.

(c)

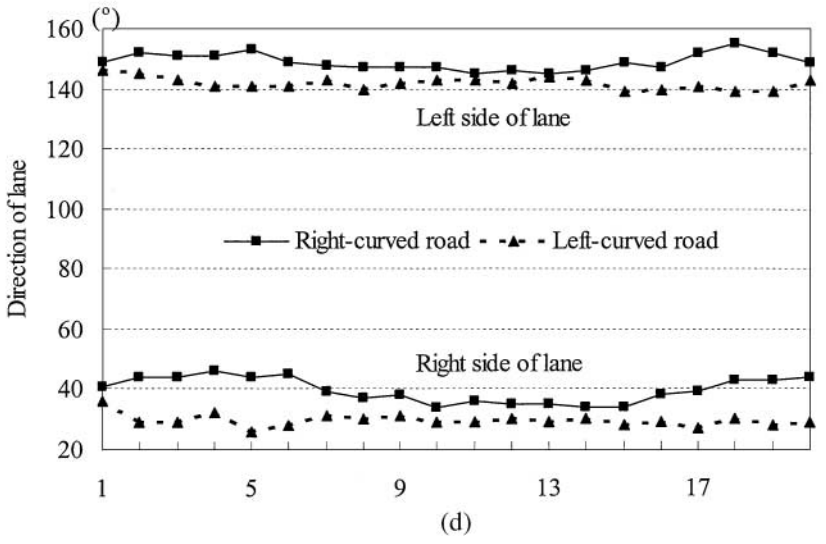

(d)

FIG. 10—*Continued*

chord from the center of the circle is 1.44 m, which is nearly half of the width of the lane. According to this analysis, the EDF-based approach to detect a lane-departure may produce a false alarm or a miss-detection on the roads with a permitted velocity less than 60 km/h such as type-4 and type-5 roads.

Figure 11 shows that the EDF generally provides distinctive peak points even if the lane direction is curved, except for a sharp curved road such as a ramp. Figure 11a illustrates an example of a highway and Fig. 11b is for a narrow rural road which provides the desirable EDF in spite of the type-4 road in Table 1 because it has a smoothly curved lane. Unlike the assumption referred to in Section 2.1, lane marks of a ramp with a sharp curved direction

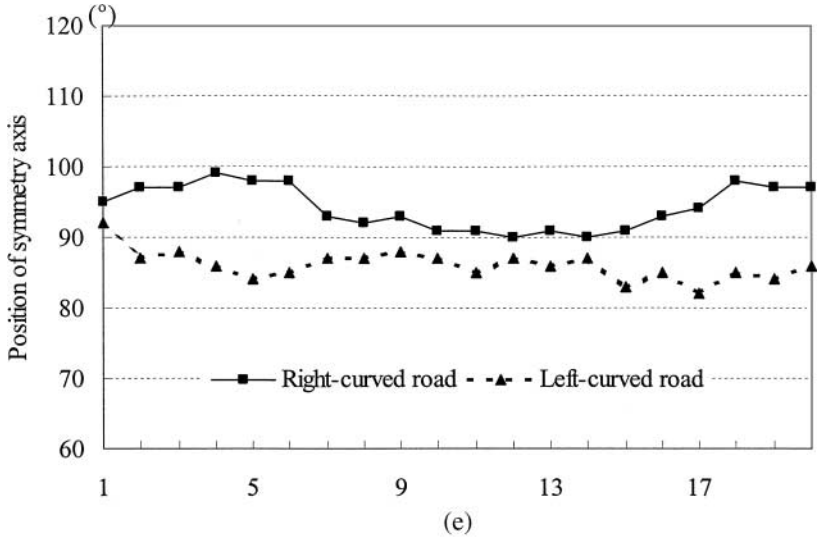

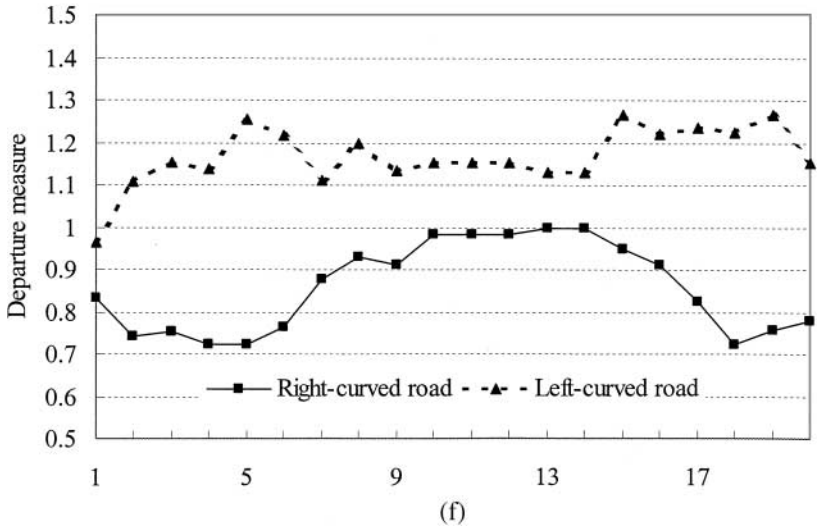

FIG. 10—*Continued*

are viewed nearly horizontal as shown in Fig. 11c. Therefore, the peaks of the EDF are close to 0° and 180°. Such EDF cannot be applied to detect a lane-departure.

Erroneous warning. We next analyze the reasons erroneous warnings occur for a curved road. Figure 12 shows consecutive images of a curved road. The lane marks on the road are evenly spaced by 10 m, which is the Korean road structure and facility criterion. Therefore, for some images, there may be no lane marks near the subject vehicle as shown in Figs. 12d and 12e. In addition, each lane mark changes in orientation in a curved road. The false alarm of lane-departure for a curved road mainly originates from these two reasons. For images in Fig. 12, we extracted the local maxima of the EDF and computed the departure measure by Eq. (12) as shown in Table 2. In the images of Figs. 12c and 12d, the orientation d_r^* changes from 42° to 49°. As the timing of the lane-departure determined by η_1 and η_2

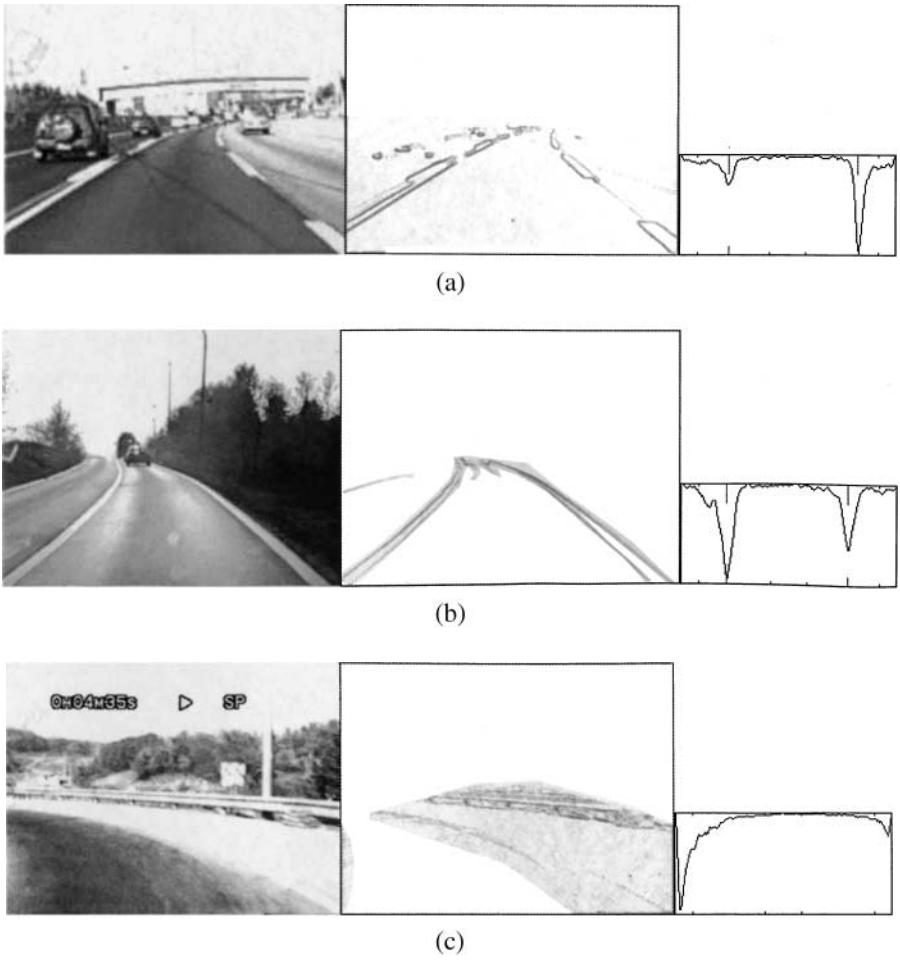

FIG. 11. Images on curved road and its EDFs: (a) A highway, (b) a narrow rural road, (c) a ramp with sharp curved direction.

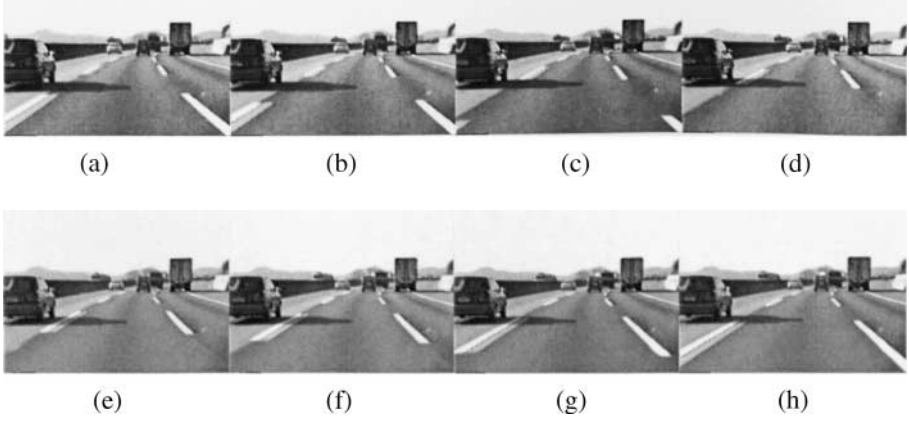

FIG. 12. Consecutive images of a curved road.

TABLE 2
The Local Maxima and Departure Measure of Images in Fig. 12

	Local maxima		
Number	d_r^*	d_l^*	Departure measure
1	38	149	0.881
2	39	150	0.85
3	42	151	0.787
4	**49**	**151**	**0.672**
5	45	151	0.738
6	42	152	0.774
7	42	151	0.787
8	43	152	0.758

of Eq. (12), we selected the values of $\eta_1 = 1.3$ and $\eta_2 = 0.7$ experimentally. According to these values, the fourth image in Fig. 12 becomes the target of a departure warning. This is just the false alarm.

6.2. Noisy Source

Although there seldom exist noisy sources satisfying the assumptions of lane marks, the shadow of a guardrail and the tracks on a worn-out road surface are given as the typical noisy factors satisfying the assumptions. In addition, according to the Korean road structure and facility criterion, the width of painted lane marks is 15 to 20 cm. This criterion, however, is often not maintained. A good example for these noisy factors is shown in Fig. 13, in which the shadow of a guardrail and the tracks of a worn-out surface are presented, and the lane marks of right lane boundary are thicker than the criterion permits. In Fig. 13c, the shape of

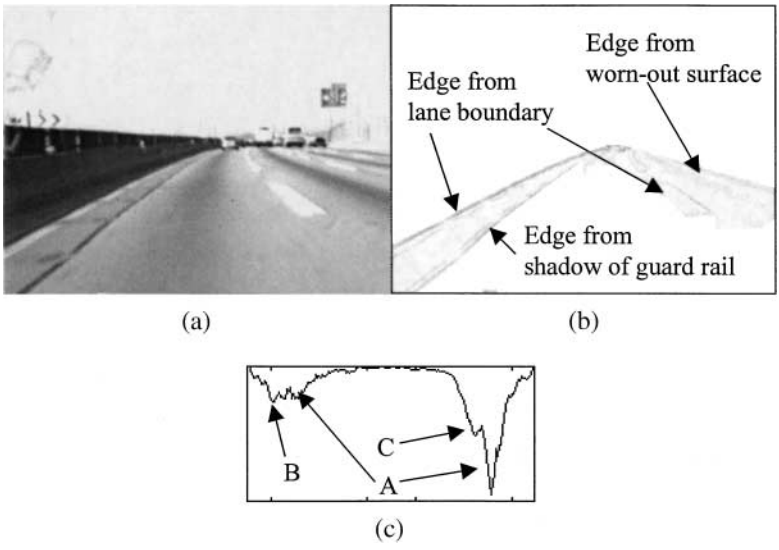

FIG. 13. A EDF from noisy image due to shadow of guardrail and worn-out surface. (a) Raw image. (b) Edge image and its sources. (c) EDF.

the EDF denoted by A was formed by edges from lane boundaries and the shapes denoted by B and C are formed by edges from the tracks of a worn-out surface and edges from the shadow of a guardrail, respectively. As these factors make the shape of the EDF thick and have multiple peaks, and continue for a long time, it is difficult to extract the correct local maxima of the EDF.

Figure 14 shows the other noisy factors in road images. Figures 14a to 14c are images of a rainy day. The aim of these figures is to show that under the same adverse situation the results may be different. In the first two images, lane marks come into view and the EDFs produce comparatively distinctive peak points, whereas in the third image, the lane marks are nearly invisible and the EDF does not produce distinctive peak points. In Fig. 14d, the EDF has distinct peak points in spite of shadows on the road from trees and mountains because the lane marks are visible. Figure 14e illustrates an image of a traffic jam, in which no lane marks come into view due to the occlusion by the truck in front. Eventually, the EDF does not provide distinct peaks in the position of expectation. The images in Fig. 14 show that the EDF-based approach to detect lane-departure highly depends on the visibility

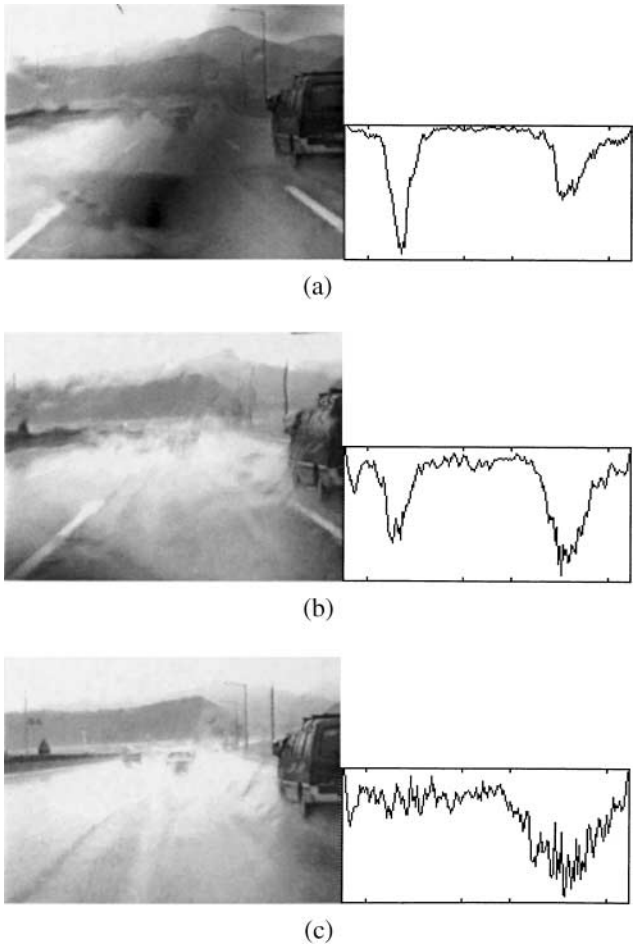

FIG. 14. Noisy images and their EDFs. (a)–(c) Noisy images on a rainy day. (d) A noisy image by a shadow. (e) A noisy image by an occlusion.

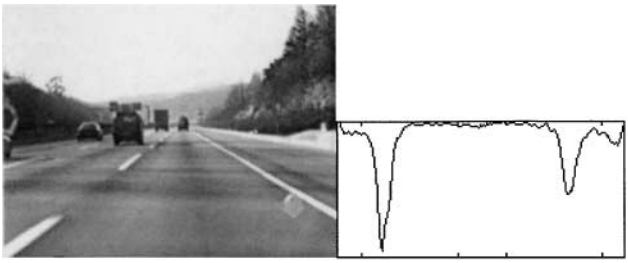

(d)

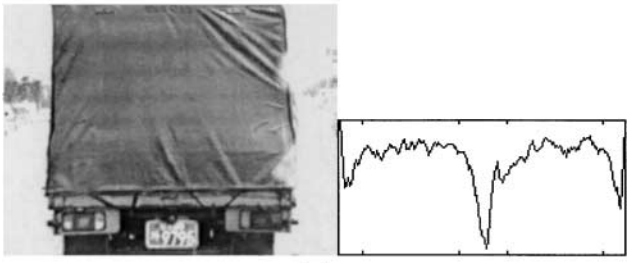

(e)

FIG. 14—*Continued*

of lane marks. Accordingly, prior to the detection of lane-departure the visibility of lane marks should be known.

6.3. A Summary of Results

For 1200 image frames obtained on a highway within the range of 2 km in which straight, right-curved, and left-curved lanes are included, the departure measure of Eq. (12) was computed and showed in Fig. 15. The image frames were composed of 408 frames (frame

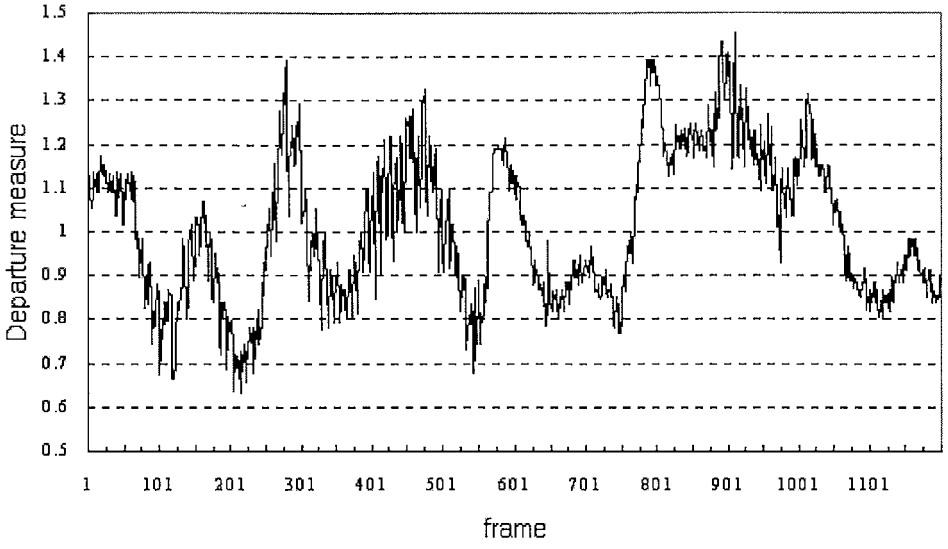

FIG. 15. A graph of departure measures.

TABLE 3
False Alarm and Miss-Detection for Entire Frames

	Ground truth	
Extraction	No departure	Departure
No departure	1128 frames (96.4%)	1 frame (3.3%)
Departure	42 frames (3.6%)	29 frames (96.7%)

TABLE 4
False Alarm and Miss-Detection for Frames of Straight Lane

	Ground truth	
Extraction	No departure	Departure
No departure	408 frames (100%)	0 frame
Departure	0 frame	0 frame (100%)

TABLE 5
False Alarm and Miss-Detection for Frames of Right-Curved Lane

	Ground truth	
Extraction	No departure	Departure
No departure	497 frames (96.5%)	1 frame (16.7%)
Departure	18 frames (3.5%)	5 frames (83.3%)

TABLE 6
False Alarm and Miss-Detection for Frames of Left-Curved Lane

	Ground truth	
Extraction	No departure	Departure
No departure	223 frames (90.3%)	0 frame
Departure	24 frames (9.7%)	24 frames (100%)

numbers 1∼20, 542∼760, and 1032∼1200) of the straight lane, 521 frames (frame numbers 21∼541) of the right-curved lane, and 271 frames (frame numbers 761∼1031) of the left-curved lane. In order to demonstrate the performance of the proposed algorithm, we obtained the false alarm rate and the miss-detection rate for entire image frames, image frames from the straight lane, image frames from the right-curved lane and image frames from the left-curved lane as shown in Tables 3–6, respectively. For entire frames, the false alarm rate was 3.6% and the miss-detection rate was 3.3% as shown in Table 3. For image frames from the straight lane, the false alarm rate was 0% and the miss-detection rate was 0% as shown in Table 4. For image frames from the right-curved lane, the false alarm rate was 3.5% and the miss-detection rate was 16.7% as shown in Table 5. For image frames from the left-curved lane, the false alarm rate was 9.7% and the miss-detection rate was 0% as shown in Table 6.

Compared to the right-curved lane, the false alarm rate in the left-curved lane was higher. This was due to the deviation of the subject vehicle from the center of the lane. When the subject vehicle traveled on the left-curved lane it frequently deviated from the center of lane to the left-side lane boundary.

7. CONCLUSION

The fundamental issue of a lane-departure warning system based on machine vision is to guarantee the robustness of identification of lane-departure in diverse conditions. The decision of a point of time of a lane-departure warning does not accompany a theoretical approach due to its heuristic determination by trial and error. From these points of view, the proposed system was quite successful. The performance of the algorithm has been proven through experimental results in various situations. The formulation of the EDF and its recursive estimation based on a moving sum and the establishment of a lane-departure condition based on the local maxima and the symmetry axis of the EDF were carried out to enhance the performance of the algorithm. However, the algorithm may provide erroneous results such as a false alarm or a miss-detection when a test vehicle travels on a road with a sharp curved direction and a road with severe noisy factors producing poor visibility of lane marks. We found that the EDF-based based approach to detect lane-departure depended highly on the visibility of lane marks we are going on the research to identify whether lane marks are visible. Prior to the detection of lane departure the visibility of lane marks should be known. This approach aims to prevent the proposed system working on such a road with severe noisy factors by identifying such a road in advance.

The proposed algorithm was processed at the speed of 15 frames per second on a Pentium PC (330 MHz).

REFERENCES

1. T. Zielke, M. Brauckmann, and W. V. Seelen, Intensity and edge-based symmetry detection with an application to car-following, *CVGIP: Image Understand.* **58**, 1993, 177–190.
2. D. G. Luenberger, *Introduction to Linear and Nonlinear Programming*, Addison-Wesley, Reading, MA, 1973.
3. D. A. Pomerleau and T. Jochem, Rapidly adapting machine vision for automated vehicle steering, in *IEEE Expert Intelli. Systems Appl*. April, pp. 19–27, 1996.
4. D. A. Pomerleau, *Neural Network Perception for Mobile Robot Guidance*, Kluwer Academic, Boston, 1994.
5. A. D. Bimbo, L. Landi, and S. Santini, Determination of road directions using feedback neural nets, *Signal Process.* **32**, 1993, 147–160.

6. M. Brattoli, R. Tasca, A. Tomasini, E. Chioffi, D. Gerna, and M. Pasotti, A vision-based alert system, in *Proc. IEEE Intelligent Vehicles 96*, pp. 195–200, 1996.
7. J. H. Seo, H. C. An, S. S. Jeong, and Y. G. Kong, Development of lane deviation warning and preventing system through vision system and steering control, in *1998 Seoul ITS Congress*, CD-Rom, 1998.
8. R. G. Gonzalez and R. E. Woods, *Digital Image Processing*, Addison-Wesley, Reading, MA, 1992.
9. K. Sato, T. Goto, and Y. Kubota, A study on a lane departure warning system using a steering torque as a warning signal, in *Proc. AVEC' 98*, pp. 479–484, 1998.
10. A. Broggi, A massively parallel approach to real-time vision based road marking detection, in *Proc. IEEE Intelligent Vehicles 95*, pp. 84–89, 1995.
11. M. Bertozzi and A. Broggi, Real-time lane and obstacle detection on the GOLD system, in *Proc. IEEE Intelligent Vehicles 96*, pp. 213–218, 1996.
12. O. Faugeras, *Three-Dimensional Computer Vision: A Geometric Viewpoint*, MIT Press, Cambridge, MA, 1993.
13. A. Gelb, *Applied Optimal Estimation*, MIT Press, Cambridge, MA, 1984.
14. J. D. Crisman and C. E. Thorpe, SCARF: A color vision system that tracks roads and intersections, *IEEE Trans. Robotics Automat*. **9**, 1993, 49–58.
15. J. W. Lee, K. S. Kim, S. S. Jeong, and Y. W. Jeon, Lane departure warning system: Its logic and on-board equipment (20005331), in *Proc. JSAE, Japan*, pp. 9–11, 2000.
16. J. W. Lee, U. K. Lee, and K. R. Baek, A cumulative distribution function of edge direction for road lane detection, *IEICE*, **E84-D**, 2001, 1206–1216.
17. U. Hofmann, A. Rieder, and E. D. Dickmanns, EMS-Vision: Application to hybrid adaptive cruise control, in *Proc. IEEE Intelligent Vehicles 2000*, pp. 468–473, 2000.
18. E. D. Dickmanns and A. Zapp, Autonomous high speed road vehicle guidance by computer vision, in *Proc. IFAC* 10th *Triennial World Congress*, pp. 221–226, 1987.